

IMPACT OF BOUNDARY CONDITION AND KINETIC PARAMETER UNCERTAINTIES ON NO_x PREDICTIONS IN METHANE-AIR STAGNATION FLAME EXPERIMENTS

Antoine Durocher
McGill University
Montréal, Québec, Canada

Gilles Bourque
ASME Fellow
Combustion Key Expert
Siemens Canada Limited

Adjunct Professor
McGill University
Montréal, Québec, Canada

Jiayi Wang
McGill University
Montréal, Québec, Canada

Jeffrey M. Bergthorson*
ASME Fellow
Professor
McGill University
Montréal, Québec, Canada

ABSTRACT

A comprehensive understanding of uncertainty sources in experimental measurements is required to develop robust thermochemical models for use in industrial applications. Due to the complexity of the combustion process in gas turbine engines, simpler flames are generally used to study fundamental combustion properties and measure concentrations of important species to validate and improve modelling. Stable, laminar flames have increasingly been used to study nitrogen oxide (NO_x) formation in lean-to-rich compositions in low-to-high pressures to assess model predictions and improve accuracy to help develop future low-emissions systems. They allow for non-intrusive diagnostics to measure sub-ppm concentrations of pollutant molecules, as well as important precursors, and provide well-defined boundary conditions to directly compare experiments with simulations. The uncertainties of experimentally-measured boundary conditions and the inherent kinetic uncertainties in the nitrogen chemistry are propagated through one-dimensional stagnation flame simulations to quantify the relative importance of the two sources and estimate their impact on predictions. Measurements in lean, stoichiometric, and rich methane-air flames are used to investigate the production pathways active in those conditions. Various spectral expansions are used to develop surrogate models with

different levels of accuracy to perform the uncertainty analysis for 15 important reactions in the nitrogen chemistry and the 6 boundary conditions (ϕ , T_{in} , u_{in} , du/dz_{in} , T_{surf} , P) simultaneously. After estimating the individual parametric contributions, the uncertainty of the boundary conditions are shown to have a relatively small impact on the prediction of NO_x compared to kinetic uncertainties in these laboratory experiments. These results show that properly calibrated laminar flame experiments can, not only provide validation targets for modelling, but also accurate indirect measurements that can later be used to infer individual kinetic rates to improve thermochemical models.

INTRODUCTION

Reducing NO and NO₂ (NO_x) emissions has become a priority in the gas turbine industry to mitigate the environmental impact of energy production and satisfy the increasingly stringent regulations on pollutant emissions. The risks and costs associated with the development of novel low-emissions combustion systems have promoted the use of numerical simulation tools in preliminary design to identify promising configurations. Predictions of NO_x emissions at elevated-pressures, however, were found to be generally inaccurate and plagued with significant uncertainties [1,2]. For these numerical tools to become predictive, a thorough understanding of uncertainty sources is necessary to

*Corresponding author. Email: jeff.bergthorson@mcgill.ca

help identify promising combustors with confidence.

Validation of thermochemical mechanisms should therefore be performed in experimental conditions that minimize systematic and random uncertainty sources, such that the discrepancies observed between experimental measurements and simulations result from modelling inaccuracies. When simulating these cases, however, uncertainties generally come from two sources: boundary conditions and kinetic modelling. The random fluctuations of the boundary conditions can have significant impact on predictions in engine-relevant operation [3], but their impact in controlled experimental facilities have not been fully quantified. Inherent modelling uncertainty arise from the choice of reactions and species included in a thermochemical mechanism and from kinetic parameters, such as specific reaction rate constants, activation energy, *etc.* Kinetic uncertainty comes from an initial lack of knowledge and it can therefore be remedied, or reduced, with additional increasingly accurate experimental measurements from the community [4, 5], independent evaluations from first principles [6], or through uncertainty quantification techniques [7]. Sampling methods, previously used to perform model optimization and uncertainty quantification [8,9], are now being replaced with advanced spectral techniques to significantly reduce computational time. The surrogate models generated with spectral expansions then provide statistics on the quantities of interest, similarly to sampling methods, but also relationships between uncertain parameters to investigate chemical modelling [7, 10, 11, 12]. Forward uncertainty propagation has been used to quantify NO prediction uncertainty in various configurations to identify problematic reactions [3, 9, 13, 14].

The interactions between the four NO_x pathways found in hydrocarbon flames [15]: thermal, prompt, N₂O, and NNH, make it difficult to isolate individual reactions to obtain direct reaction rate measurements similar to other chemical sub-models [5]. For instance, production through the NNH route occurs in the radical pool at the flame front and involves tens of reactions with some of them linked to the N₂O pathway. As such, indirect measurements have been used to investigate the nitrogen chemistry. Flow reactors [16] and laminar flames stabilized with McKenna [17, 18], jet-wall stagnation [19, 1, 20], and counterflow [21, 22] burners have been used to study NO_x formation in experiments designed to target specific production routes to provide independent experimental datasets to improve modelling. Out of the four formation routes, the thermal and prompt routes have been the focus of more experiments by increasing the contribution of each route in high-temperature environments and in hydrocarbon-fuel rich conditions, respectively.

The impact of uncertain boundary conditions and inherent kinetic uncertainty on NO_x predictions is quantified in this work for a jet-wall stagnation flame configuration. Lean-to-rich methane-air mixtures are used to assess the validity of using indirect measurements obtained with laminar flames to improve chemical modelling. Using nested sparse grid spectral expan-

sions, NO prediction uncertainties are quantified for 6 boundary conditions (ϕ , T_{in} , u_{in} , du/dz_{in} , T_{surf} , P) and 15 important reactions in the nitrogen chemistry simultaneously. The contribution of individual parameters and interactions between parameters is explored to identify dominant sources of uncertainty that would benefit from additional measurements to improve modelling.

METHODOLOGY

The experimental configuration used in this work is described in [19, 23] where quantitative measurements of NO and CH profiles are presented, respectively. The jet-wall stagnation burner shown in Fig. 1 provides stable, laminar, and lifted flames accessible for laser diagnostics with accurate experimentally-measured boundary conditions to directly compare measurements with simulations. The measured boundary conditions in a laboratory environment provide minimal uncertainty which allows for precise investigation of uncertainty sources.

Experimental apparatus

The premixed fuel-air mixture, shrouded by a co-flowing inert gas, exits the bottom nozzle in Fig. 1 and impinges on a water-cooled stagnation surface whose temperature is monitored with three K-type thermocouples throughout the experiments to prevent surface reactions. In this configuration, the flame stabilizes at the location where its propagation speed matches the velocity of the decelerating impinging flow. Flames are stabilized sufficiently upstream of the stagnation surface to exhibit nearly-adiabatic conditions. These careful considerations ensure that the measured reactivity and emissions are solely a function of the properties of the combustible mixtures. Velocity, NO concentration, and temperature profiles measured with particle tracking velocimetry, laser-induced fluorescence (LIF), and multi-line NO-LIF thermometry, respectively, provide experimental targets for model improvement.

Experimentally-measured boundary conditions provided by Watson *et al.* [19] to allow for direct simulation of the experiments are summarized in Appendix A along with their measured uncertainty. In this configuration, boundary conditions required for the stagnation surface and the gas inlet are shown in Fig. 1. By definition, there is no species flux and a null axial velocity at the wall. The temperature is carefully monitored with thermocouples to provide the wall-boundary condition. Similarly, the inlet temperature of the combustible mixture is monitored throughout the experiments with K-type thermocouples. The mixture composition is controlled by thermal mass flow controllers, calibrated with a dry-piston calibrator, that provide an accuracy of $\pm 0.7\%$ on the equivalence ratio. Velocity-boundary conditions are obtained from Particle Tracking Velocimetry (PTV) [19, 23]. A least-squares parabolic fit in the cold flow region upstream of the flame provide the inlet axial veloc-

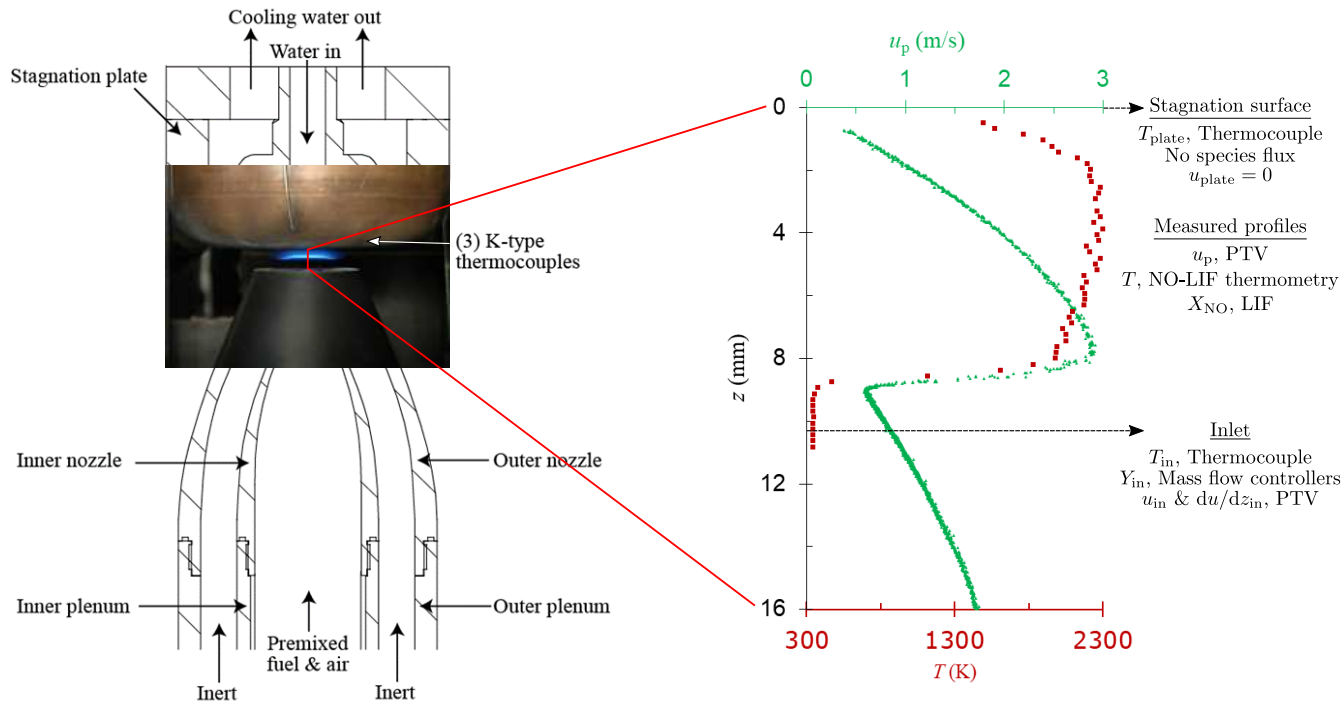


FIGURE 1. IMPINGING JET-WALL STAGNATION BURNER USED BY WATSON *ET AL.* [19]. TEMPERATURE (RED) AND VELOCITY (GREEN) PROFILES WITH ACCURATE EXPERIMENTALLY-MEASURED BOUNDARY CONDITIONS USED IN SIMULATIONS.

ity, u_{in} , and strain, du/dz_{in} . The numerical domain length, l , is measured from the stagnation surface to the axial location where the velocity-boundary conditions are measured from.

Simulations are performed with the quasi-one dimensional (1D) model provided in Cantera 2.4 [24] with the experimentally-measured boundary conditions to allow for direct comparison with the experiments. The thermochemical mechanism used in this work is assembled from the base chemistry of the 2015 San Diego mechanism [25] optimized for accurate CH chemistry [26] and the nitrogen chemistry from the NOMEcha 2.0 mechanism [18]. To ensure a systematic comparison between the lean ($\phi = 0.8$), stoichiometric ($\phi = 1.0$), and rich ($\phi = 1.3$) cases, the uncertainty in NO concentration predictions is evaluated 10 ms downstream of the flame, defined as the peak concentration of methylidyne radicals, $[CH_{peak}]$.

Probabilistic input parameter definition

The uncertainty analysis investigates the impact of 21 parameters on the predictions of NO concentrations and $[CH_{peak}]$. The six uncertain operating conditions include the equivalence ratio (ϕ), inlet temperature (T_{in}), stagnation plate temperature (T_{wall}), inlet velocity (u_{in}), inlet velocity gradient (du/dz_{in}), and ambient pressure (P). The experimentally-measured boundary conditions, along with their uncertainties, reported by Watson

and co-workers [19], are used to bound the analysis. The uncertainty in these parameters mostly results from random fluctuations in the measuring equipment and are therefore assumed to be randomly distributed around their averaged value.

The remaining 15 uncertain parameters are the specific reaction rate constants of reactions having both a high uncertainty and a large impact on NO formation, as identified with uncertainty-weighted sensitivity analysis in [14]. The entire thermochemical mechanism is analysed through the uncertainty-weighted sensitivity analysis. The important reactions identified through this process do not include reactions from the NNH and N_2O pathways as the experiments considered mostly attempt to isolate the contributions of the thermal and prompt routes through the high-temperature atmospheric flames and the rich flame, respectively. The upper and lower uncertainty limits, expressed with the multipliers $1/f_{i,low}$ and $f_{i,high}$, from [14] bound the uncertainty of the kinetic domain. Since the data is too sparse to derive any meaningful statistics for the rate constants, uniform distributions are used in this analysis.

Spectral expansion

Spectral expansion is used to obtain a surrogate model that describes the relationship of the desired response variable as a function of the uncertain parameters. Similarly to a Fourier

expansion for periodic signals, a polynomial chaos expansion (PCE) captures the response variable R with respect to the input parameters \mathbf{x} with orthogonal polynomial combinations. The complete expansion is presented in Eq. 1 where R_0 is a constant, α are real coefficients, and P_i is the orthogonal polynomial basis of interaction order i . It can be written in a compact form in Eq. 2 with multivariate polynomials Ψ_i .

$$R(\mathbf{x}) = R_0 + \sum_{k_1=1}^{\infty} \alpha_{k_1} P_1(x_{k_1}) + \sum_{k_1=1}^{\infty} \sum_{k_2=1}^{\infty} \alpha_{k_1, k_2} P_2(x_{k_1}, x_{k_2}) \quad (1)$$

$$\begin{aligned}
 &+ \sum_{k_1=1}^{\infty} \sum_{k_2=1}^{\infty} \sum_{k_3=1}^{\infty} \alpha_{k_1, k_2, k_3} P_3(x_{k_1}, x_{k_2}, x_{k_3}) \dots, \\
 &= R_0 + \sum_{k=1}^{\infty} \alpha_k \Psi_k(\mathbf{x}) = \sum_{k=0}^{\infty} \alpha_k \Psi_k(\mathbf{x}). \quad (2)
 \end{aligned}$$

For practical considerations, the expansion is truncated to the desired polynomial order p where the number of terms in the expansion, K , depends on the number of parameters, the maximum polynomial order, and the spectral technique selected.

$$R(\mathbf{x}) \approx R_0 + \sum_{k=1}^K \alpha_k \Psi_k(\mathbf{x}) = \sum_{k=0}^K \alpha_k \Psi_k(\mathbf{x}). \quad (3)$$

Known polynomial bases corresponding to specific distributions are used in the expansion, Legendre and Hermite polynomials for uniform and normal distributions [27], respectively. The coefficients can then be evaluated using regression, or spectral projection on the orthogonal polynomial basis functions with

$$\alpha_k = \frac{\langle R, \Psi_k \rangle}{\langle \Psi_k, \Psi_k \rangle} = \frac{1}{\langle \Psi_k, \Psi_k \rangle} \int_{\Gamma} R(\mathbf{x}) \Psi_k(\mathbf{x}) \rho_{\mathbf{x}}(\mathbf{x}) d\mathbf{x}, \quad (4)$$

where $\rho_{\mathbf{x}}$ is the joint probability density of the input parameters, and Γ is the interval for integration or sample space. For complex multivariate systems, the integral is calculated numerically. The numerical integration and surrogate model development are performed with Dakota [28] using the framework from [14]. Details on the derivation of the integration can be found for various spectral collocation techniques in [29, 30]. The development of the numerical integration for the two strategies considered in this work to evaluate the coefficients of the expansion, the total-order and tensor-product expansions, can be found in [14] while key differences between the methods are summarized here.

The **total-order expansion** can be considered one of the simplest technique to evaluate the polynomial coefficients. It bounds the maximum order of the response surface with the prescribed order p resulting in a linear response surface for a 1st-

order expansion, a quadratic response surface for a 2nd-order expansion, *etc.* A Monte Carlo integration is often used to evaluate the integral. Random collocation points in the uncertain domain are evaluated to constrain the K terms of the expansion and polynomial coefficients can be obtained via regression or Eq. 4. Advanced sampling techniques, such as Latin Hypercube Sampling, can be used to improve the accuracy of the surrogate model over a traditional random sampling. This technique requires a minimum of K collocation points to develop the surrogate model, but will benefit from additional samples to provide a better coverage of the entire uncertain domain. With the 21 parameters selected, 253 collocation points are required for a 2nd-order expansion.

The **tensor-product expansion** uses deterministic quadrature methods instead of random sampling. Contrary to total-order expansions, tensor-product methods do not limit the maximum order of the polynomials, but rather limit the number of variables in multivariate terms of the expansion. Consequently, for a level 1 expansion, ℓ_1 , the terms of the expansion would contain up to one parameter, for a ℓ_2 expansion there would be up to two parameters per term, *etc.* In this case, the order of the expansion is determined by additional considerations such as the recursiveness of the technique or the shape of the structured grid.

Nested sparse grids are used in this work to develop the surrogate models. This technique contains a subset of collocation points from the tensor-product expansion that was proposed to alleviate the high computational costs of the full tensor-product expansion while retaining its accuracy in high-dimensional problems [31]. Most of the analysis in this work is performed with a ℓ_2 nested sparse grid formulation. The response surfaces developed under this approach yield polynomials reaching a 5th-order approximation for single parameters and pairwise, or two variables, interactions up to the 4th-order. In this case, 979 collocation points are required to develop the surrogate models.

Parametric contribution analysis

Specific polynomial bases are associated with each parameter distribution. For the normally distributed boundary conditions and the uniformly distributed kinetic parameters, probabilist Hermite and Legendre polynomials are used, respectively [27]. The first three non-constant basis functions are given in Table 1.

TABLE 1. POLYNOMIAL BASIS FUNCTIONS.

Hermite (Normal)	Legendre (Uniform)
$P_1(x) = x$	$P_1(x) = x$
$P_2(x) = x^2 - 1$	$P_2(x) = (x^3 - 1)/2$
$P_3(x) = x^3 - 3x$	$P_3(x) = (5x^3 - 3x)/2$

Normalized variables are used in the expansion. Normally-distributed parameters have a mean of 0 and a standard deviation of 1.

tion of 1 and uniformly-distributed ones are bounded between -1 and 1 . By definition, the mean of the surrogate model is then equal to the constant term R_0 . Every αP term of the expansion in Eq. 1 can be viewed as a deviation from the mean R_0 . If all the polynomials are from the same family, only Hermite for instance, the relative contribution from each term can be determined by directly comparing the magnitude of the coefficients α [10]. When multiple polynomial bases with different order are used in the expansion, the entire term αP needs to be considered. The contribution of single parameters, c_{x_i} , and groups of parameters, c_{x_i, x_j} are assembled in Eqs. 5 and 6 to evaluate the impact of single parameters and parameter interactions.

$$c_{x_i} = \alpha_i P_1(x_i) + \alpha_{i,i} P_2(x_i) + \dots \quad (5)$$

$$c_{x_i, x_j} = \alpha_{i,j} P_2(x_i, x_j) + \dots \quad (6)$$

By definition, the expectation of every contribution c is null and its standard deviation estimates the impact to global uncertainty. For systematic comparison between parameters in the expansion, the contributions c are normalized by the mean response of the surrogate model, R_0 , before the standard deviation is evaluated by sampling over S independent sets of parameters with

$$\sigma_{c_{x_i}} = \sqrt{\frac{\sum_{s=1}^S (c_{x_i, s}/R_0)^2}{S}}, \quad (7)$$

RESULTS

Demonstration of contribution analysis for $\phi = 0.8$

The contribution analysis is first performed for the lean, $\phi = 0.8$, methane-air flame to demonstrate the processing steps to obtain contribution grids. A level-2, ℓ_2 , nested sparse grid with 979 simulation points is used to generate the surrogate model. Peak concentrations of methylidyne radicals, $[\text{CH}_{\text{peak}}]$, and NO concentrations are extracted from the surrogate model. NO concentrations are evaluated 10 ms downstream of the flame front, defined as the location of $[\text{CH}_{\text{peak}}]$, to achieve residence times comparable to gas turbine architectures. The PDF evaluating the uncertainty on NO prediction is shown in Fig. 2 where the width of the distribution corresponds to the prediction uncertainty. The effect of different uncertainty sources, from boundary conditions and kinetic parameters, on predictions is explored by activating specific sections of the polynomial expansion and are shown in Fig. 2 against the complete response.

The impact of boundary condition uncertainties are shown to have a minimal effect of the prediction of NO molecules as observed by the narrow distribution. Although the experiment is very sensitive to some boundary conditions, such as ϕ and inlet temperature, the narrow operating uncertainties on the equipment

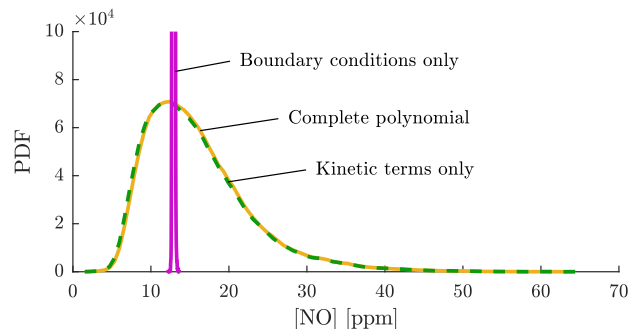


FIGURE 2. [NO] DISTRIBUTIONS AT $\phi = 0.8$ FOR THE COMPLETE EXPANSION (—), BOUNDARY CONDITIONS ONLY (—), AND KINETIC PARAMETERS ONLY (---).

mitigate their impact on predictions. Contrary to industrial applications where the boundary condition uncertainty is expected to be around 4% [3], the impact of fluctuating boundary conditions is minimized in this controlled setting where the uncertainty is generally below 1%. The PDF accounting for chemical kinetic contributions only, however, is almost identical to the result obtained from the complete polynomial description. These results suggest that the chemical kinetic terms cause almost all the NO uncertainty in this experiment, with little impact from the uncertain boundary conditions. Consequently, laminar flame experiments with well-defined experimentally-measured boundary conditions provide ideal configurations to obtain data of key combustion parameters. Since NO concentration measurements have a 95% confidence interval of approximately 15%–20% in this experimental apparatus, depending on operating conditions, and the $\pm 2\sigma$ prediction interval covers $[-53\%, +131\%]$ of the average value, stagnation flame experiments can produce useful data to improve kinetic modelling using indirect measurements.

The major sources of uncertainties are identified by grouping the contribution of individual parameters. For this analysis with 6 uncertain boundary conditions and 15 uncertain specific reaction rate constants, the polynomial expansion becomes

$$R(\mathbf{y}, \mathbf{z}) = R_0 + \sum_{k_1=1}^6 c_{y_{k_1}} + \sum_{k_1=1}^6 \sum_{k_2=1}^6 c_{y_{k_1}, y_{k_2}} \quad (8)$$

$$+ \sum_{m_1=1}^{15} c_{z_{m_1}} + \sum_{m_1=1}^{15} \sum_{m_2=1}^{15} c_{z_{m_1}, z_{m_2}}$$

$$+ \sum_{k_1=1}^6 \sum_{m_1=1}^{15} c_{y_{k_1}, z_{m_1}},$$

where the terms are grouped with respect to boundary conditions, y_k , kinetic parameters, z_m , and their combinations. The ℓ_2 sparse grid only considers pairwise parameter interactions, leading to

the double-summation grouped terms in Eq. 8 for interactions between 1) boundary condition - boundary condition, 2) rate constant - rate constant, and 3) boundary condition - rate constant.

The sums of the contribution values of the boundary conditions, the reaction rate constants, and their interactions to the prediction uncertainty on NO concentrations are compared using $\sigma_{c_{x_i}}$, defined in Eq. 7. The relative importance of the contribution of each group is evaluated with respect to the uncertainty from the complete surrogate model predictions. For the lean flame, the boundary conditions, kinetic parameters, and their interactions contribute to 2%, 95%, and 3%, respectively, of the NO prediction uncertainty. These results are expected from the PDF comparison presented in Fig. 2, where the narrow distribution of the boundary conditions suggested a negligible contribution. Similarly, interactions between the two sources of uncertainties lead to negligible impact on the prediction as well.

The contribution values of individual variables can be decomposed as well from Eq. 7. Individual parametric contributions are visualized in Fig. 3 for the 21 parameters studied. Since the contribution matrices are symmetric, the upper right triangular region presents the impact of uncertainty sources on the $[\text{CH}_{\text{peak}}]$ while the bottom left triangle shows the impact on NO concentration. This visualization allows for rapid identification of important relationships between the two quantities of interest, where the colour intensity of each square represents the amount of contribution from the corresponding variable towards the output variable uncertainty. In this representation, the diagonal cor-

responds to direct impact of a given uncertain parameter to the global uncertainty, while off-diagonal terms present the impact of pairwise polynomials, or cross-term interactions.

In these laboratory experiments, the kinetic uncertainty dominates the variability in both, NO and $[\text{CH}_{\text{peak}}]$. For the lean flame, the uncertainty in NO prediction is distributed between the thermal and prompt formation mechanisms. Unsurprisingly, the reactions greatly affecting the formation of CH in turn affect the NO formation through the prompt pathway. Although the initiation reaction, $\text{CH} + \text{N}_2 \rightleftharpoons \text{H} + \text{NCN}$, greatly affects prediction uncertainty, the pairwise interactions with other reactions involving CH present significant contributions to the uncertainty. This supports the discussion by Versailles *et al.* about the need for an adequate description of the CH chemistry to accurately capture NO formation [23]. Since CH is considered to be present in quasi-steady state in the flame, individual reactions involved with CH greatly affect the global concentration present in the flame and, consequently, the prompt-NO formation.

Impact of uncertainties in lean-to-rich flames

The individual parametric contributions for the stoichiometric, $\phi = 1.0$, and rich, $\phi = 1.3$, methane-air flames are presented in Figs. 4 and 5, respectively. Similarly to the lean case, the uncertainty in both quantities of interest is dominated by the inherent uncertainty of the thermochemical mechanism. The relative impacts of the grouped contribution values on NO uncertainty are compared in Table 2 for the lean-to-rich cases. The stoichiometric flame presents the largest impact of boundary conditions. In this case, the equivalence ratio has a greater impact on the solution since small fluctuations can lead to different behaviour whether these fluctuations in the equipment push the mixture on the lean or rich side. Nonetheless, the uncertainty in boundary conditions only corresponds to 4% and the kinetic uncertainty dominates the contribution to prediction uncertainties.

A comparative inspection of Figs. 3, 4, and 5 for the lean, stoichiometric, and rich cases, respectively, show differences in the parameters contributing to the prediction uncertainty of both NO concentration and $[\text{CH}_{\text{peak}}]$. In the stoichiometric case, the thermal initiation reaction $\text{N}_2 + \text{O} \rightleftharpoons \text{N} + \text{NO}$ is the most important uncertainty source while both the thermal and prompt routes had a similar contribution in the lean case. The stoichiometric post-flame temperature is higher than the lean mixture, approximately 2200 K compared to 1980 K, leading to a faster reaction rate for the rate-limiting step of the thermal mechanism. Consequently, the specific reaction rate constant uncertainty will have a greater impact on the prediction as a small change can lead to large prediction discrepancies because of the exponential dependency of temperature in the Arrhenius description of the reaction. The thermal initiation reaction contribution then rapidly decreases in the rich mixture. The formation pathway is rapidly inhibited by the oxygen-deprived environment to the point where

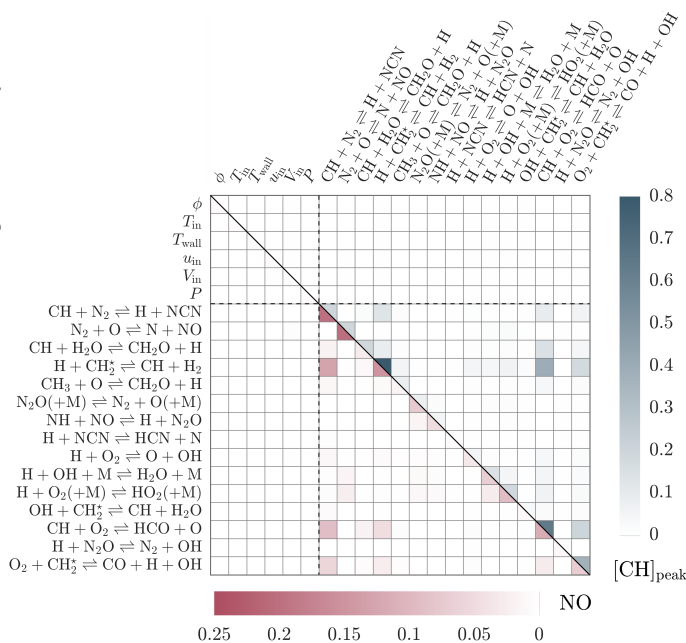


FIGURE 3. CONTRIBUTION TO NO (■) AND CH (■) UNCERTAINTIES USING l_2 SPARSE GRID FOR $\phi = 0.8$ CONDITIONS.

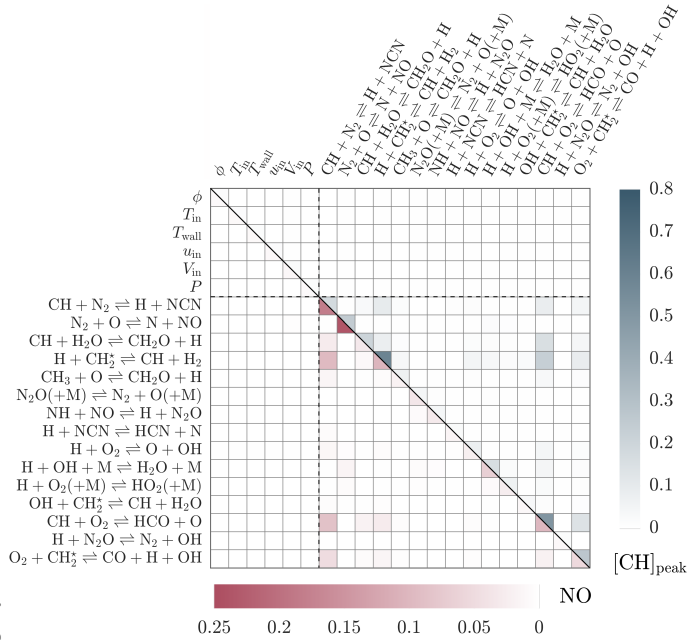


FIGURE 4. CONTRIBUTION TO NO (■) AND CH (■) UNCERTAINTIES USING ℓ_2 SPARSE GRID FOR $\phi = 1.0$ CONDITIONS.

the thermal pathway does not contribute to the predicted emissions of NO, as expected.

The prompt-NO pathway is shown to be important in the three mixtures considered. From an even contribution to NO in lean flames, the contribution of the prompt-NO pathway to uncertainty decreases slightly in the stoichiometric mixture before becoming the sole source of uncertainty in the rich flame with a kinetic uncertainty representing 98% of the global NO uncertainty. In rich conditions, it is expected that the sole NO prediction uncertainty comes from the prompt pathway since it is generally the only formation route considered active in rich methane-air flames. Among the CH chemistry, the rate-limiting initiation reaction $\text{CH} + \text{N}_2 \rightleftharpoons \text{H} + \text{NCN}$ is the dominant contributor to prediction uncertainty. It is important to note that the direct contribution of this reaction alone increases the uncertainty by approximately 75% of the predicted average in both quantities of interest. For the rich flame, the remaining NO uncertainty

TABLE 2. CONTRIBUTION TO NO PREDICTION UNCERTAINTY USING ℓ_2 SPARSE GRIDS.

ϕ	$\frac{\sum \sigma_{\text{BC}}}{\sum \sigma}$	$\frac{\sum \sigma_{\text{kin}}}{\sum \sigma}$	$\frac{\sum \sigma_{\text{BC,kin}}}{\sum \sigma}$
	0.8	2%	95%
1.0	4%	92%	4%
1.3	1%	98%	1%

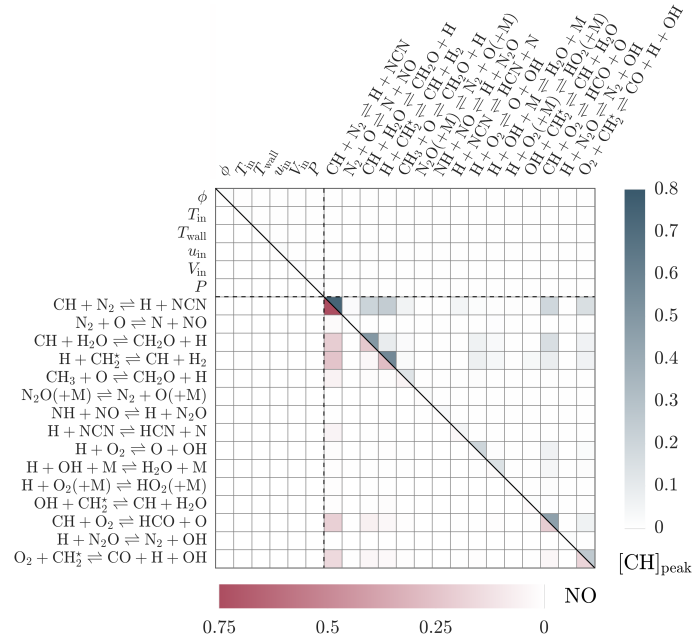


FIGURE 5. CONTRIBUTION TO NO (■) AND CH (■) UNCERTAINTIES USING ℓ_2 SPARSE GRID FOR $\phi = 1.3$ CONDITIONS.

arises mostly from pairwise interactions between reactions that greatly impact the peak CH concentration. A similar behaviour is observed for the CH prediction uncertainty, as expected, since the uncertainties in the CH chemistry have been shown to propagate through the nitrogen chemistry while being amplified via the prompt initiation reaction [14].

Contribution of interacting and higher-order terms

In the three cases studied, a majority of the off-diagonal elements are blank, indicating a generally small effect of interactions between uncertain parameters. The only terms that exhibit strong pairwise impacts are reactions competing for the same reactants, such as CH. The boundary conditions do not have a significant contribution directly or through interactions with chemical kinetic variables in the cases studied experimentally. This observation suggests that modelling parameter interactions do not provide substantially different prediction uncertainties. In cases where a rapid uncertainty estimate is required, or encouraged, developing a surrogate model for the direct impact, in other words the diagonal of the contribution grids, would result in an acceptable estimate at reduced costs. The impact of direct and interacting terms is studied by isolating their contributions from the polynomial expansion. The analysis is also performed with a ℓ_3 nested sparse grid formulation to explore the impact of higher-order polynomial bases and three-parameter interactions.

The relative contribution of the direct and pairwise interactions to NO prediction uncertainties are presented in Table 3 for

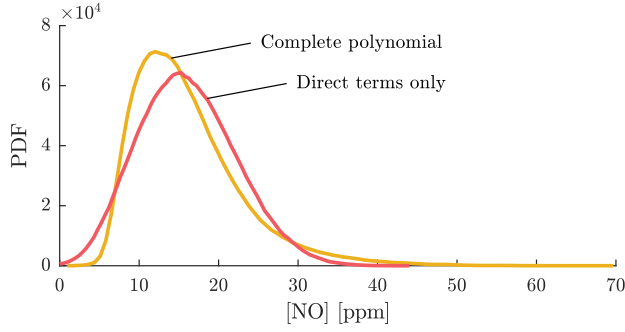


FIGURE 6. [NO] DISTRIBUTIONS OBTAINED WITH ℓ_2 SPARSE GRIDS AT $\phi = 0.8$ FOR THE COMPLETE EXPANSION (—) AND DIRECT TERMS ONLY (—).

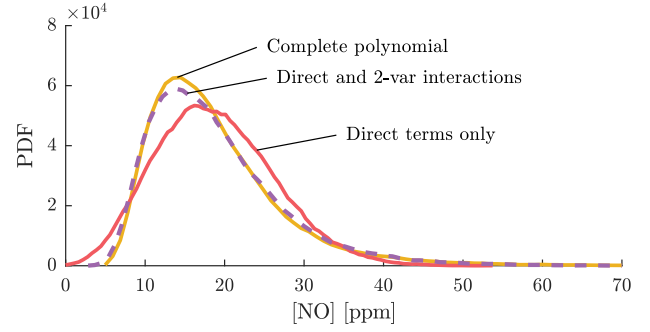


FIGURE 7. [NO] DISTRIBUTIONS OBTAINED WITH ℓ_3 SPARSE GRIDS AT $\phi = 0.8$ FOR THE COMPLETE EXPANSION (—), DIRECT AND 2-VARIABLE INTERACTION TERMS ONLY (---), AND DIRECT TERMS ONLY (—).

the lean, stoichiometric, and rich mixtures. For the conditions examined, the pairwise interaction of uncertain parameters approximately contributes 40% to the prediction uncertainty. Although the contribution value is large, the PDFs of the predicted NO concentrations shown in Fig. 6 for the complete polynomial expansion and the direct term subset exhibit relatively good agreement. Both distributions have similar widths, but the complete description has a more refined distribution with sharp increases in probability on each side of the most probable concentration. These results suggest that the interaction terms act along the direct behaviour while subtly modifying the general shape of the distribution. It is expected that interactions between parameters would not completely change the distribution, but the differences in PDFs are not as large as the 40% contribution values suggested. Consequently, the direct relationship between a parameter and the NO concentration can be estimated at reduced costs for rapid quantification of uncertainty in predictions in experimental facilities.

A similar analysis is performed using a surrogate model developed with a ℓ_3 sparse grid to quantify the impact of high-order polynomial development and three-parameter interactions. The response surface is obtained for the lean case, $\phi = 0.8$, and requires 15,579 simulation points. The PDFs of the complete polynomial description and its components are presented in Fig. 7. The direct and pairwise parameter interactions extracted from

TABLE 3. CONTRIBUTION OF DIRECT AND MIXED TERMS TO NO PREDICTION UNCERTAINTY USING ℓ_2 SPARSE GRIDS.

ϕ	$\frac{\sum \sigma_{\text{direct}}}{\sum \sigma}$	$\frac{\sum \sigma_{\text{inter.}}}{\sum \sigma}$	NO _{direct} Avg. \pm Std.	NO _{complete} Avg. \pm Std.
0.8	61%	39%	16.1 \pm 6.1	16.1 \pm 6.8
1.0	63%	37%	67.5 \pm 23.8	67.5 \pm 25.9
1.3	57%	43%	66.5 \pm 58.1	66.3 \pm 64.7

the complete ℓ_3 surrogate model present similar distributions to the ones obtained with the ℓ_2 approach in Fig. 6, as expected. The addition of the third level in the nested sparse grid formulation results in minimal changes to the distribution, with only slightly stretching the peak of the distribution. For this particular model, the direct terms have a contribution of 35%, the two-parameter interaction terms 43%, and the three-parameter interaction terms 22%. Although the three-parameter interaction terms have a contribution value of 22%, it does not seem to have significantly impacted the width of the PDF. As suggested before, the additional terms in the polynomial description only favour behaviours already observed in the direct description; increasing the peak probability and shaping the distribution towards the most probable concentration. The small difference between the PDFs generated by the polynomial with and without three-parameter interactions does not seem to justify the significantly higher computational cost to model three-parameter interactions with 15,579 simulations compared to the 979 required for ℓ_2 sparse grid. The two-parameter interactions are sufficient to capture the main characteristics of the distributions of NO and [CH_{peak}], while keeping the computational cost low.

Inadequacy of low-order analysis

The lean analysis is also performed with a traditional total-order expansion commonly used to quantify uncertainties. A 2nd-order expansion providing pairwise parameter interactions is obtained from 253 collocation points. A comparison between PDFs generated from the tensor-product ℓ_2 sparse grid and the 2nd-order total-order expansion is shown in Fig. 8 for $\phi = 0.8$. The total-order expansion surrogate model is observed to have a wider probability distribution, which is consistent with observations from [14]. A larger difference between the complete expansion and the contribution of the direct terms than the ℓ_2 sparse grid (Fig. 6) is observed. In the total-order expansion, the interacting terms are significantly pulling the NO concentration

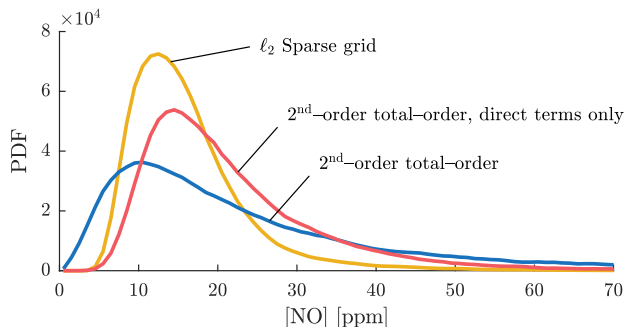


FIGURE 8. [NO] DISTRIBUTIONS AT $\phi = 0.8$ OBTAINED WITH ℓ_2 SPARSE GRIDS FOR THE COMPLETE EXPANSION (—) AND WITH 2nd-ORDER TOTAL-ORDER EXPANSION FOR THE COMPLETE EXPANSION (—) AND DIRECT TERMS ONLY (—).

predictions closer to zero while extending the distribution tail to higher concentration values. Interestingly, the interaction terms contribute to 84% of the uncertainty with the total-order expansion compared to 39% with the ℓ_2 sparse grid.

An individual contribution analysis of the 2nd-order total-order expansion is shown in Fig. 9. At first glance, the results look completely different from the sparse grid approach. Compared to the grid plot presented in Fig. 3, the interaction terms in the total-order expansion have a larger relative contribution to NO and peak CH uncertainty, as shown by the off-diagonal coloured elements. These individual contributions completely differ from the more accurate tensor-product expansions used previously with ℓ_2 and ℓ_3 nested sparse grids. It suggests that although the distributions are similar in shape and most probable prediction, the underlying surrogate model is unable to accurately capture the expected behaviour of the problem studied. The ℓ_2 sparse grid technique offers higher-order polynomials in both single parameter and pairwise parameter interactions than the 2nd-order total-order expansion. As such it exhibits a greater accuracy in capturing the non-linearities in the surrogate model and it better captures the relationship between parameters. The 2nd-order total-order captures the overall shape of the distribution, and the biggest contributors adequately, as shown by the darker elements in Fig. 9. However, the lighter elements in the contribution plot suggest an inaccurate response surface in comparison to the higher-order ℓ_2 sparse grid technique. The inadequacy of the 2nd-order total-order expansion to capture parameter relationships is visible in the individual contribution grid as there seem to be no structured relationship identified where prominent interactions should be present between reactions sharing the same species, at least. For uncertainty quantification problems focusing on NO and CH formation, advanced sparse grid expansions are then recommended to capture appropriate relationship between variables at a reasonable cost to ensure that model optimizations are properly constrained.

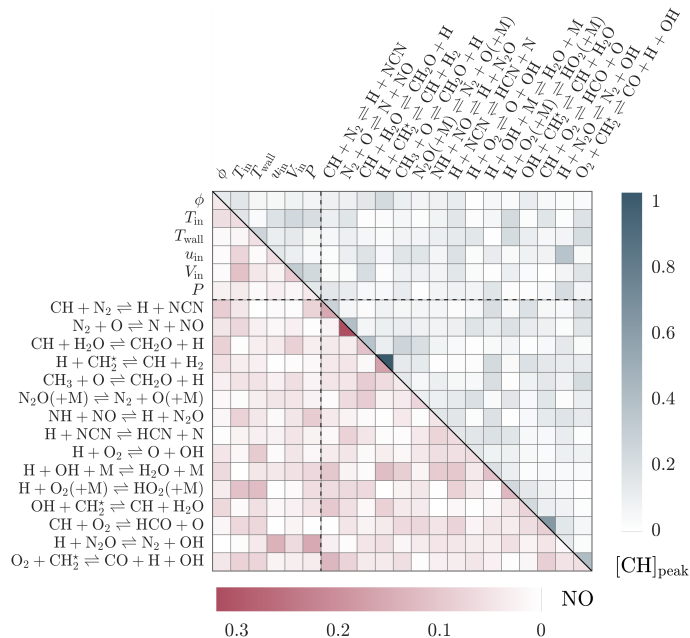


FIGURE 9. CONTRIBUTION TO NO (■) AND CH (■) UNCERTAINTIES FROM EACH INPUT VARIABLE BY ANALYSING THE POLYNOMIAL CONSTRUCTED USING SECOND-ORDER TOTAL-ORDER EXPANSION FOR $\phi = 0.8$ CONDITIONS.

CONCLUSION

The impact of uncertain boundary conditions and kinetic parameters are investigated in this work to determine the main source of uncertainty in NO and CH concentration predictions for an experimental laminar stagnation flame facility. Prediction uncertainties are quantified for lean-to-rich methane-air flames using a nested ℓ_2 sparse grid methodology to characterize the relationship between the 6 boundary conditions and the 15 specific reaction rate constants selected for the analysis. Experimentally-measured boundary conditions with their uncertainties are used in this work to assess if laminar flame experiments can improve kinetic modelling through indirect measurements.

Inherent uncertainties in the thermochemical mechanism used in this work are shown to have a significantly larger effect on predictions of both NO and CH concentrations than the uncertain experimental boundary conditions. The contribution of individual parametric sources is obtained to identify the dominant sources of uncertainty, whether it comes directly from a single parameter or from interactions between multiple parameters. The metric, the contribution value to global uncertainty, is calculated for the lean, stoichiometric, and rich cases ($\phi = 0.8, 1.0, 1.3$) studied here and the direct kinetic contribution amounts to 95%, 92%, and 98%, respectively. The predicted uncertainty interval arising from kinetic parameter is then almost an order of magnitude larger than the measured uncertainty on NO concentra-

tion measurements. These results confirm that laminar stagnation flame experiments conducted with accurate experimentally-measured boundary conditions can provide indirect measurements to validate and improve kinetic modelling.

The contribution to global uncertainty is also decoupled between pairwise parametric interactions and direct impact of single parameters for the three equivalence ratios. The results suggest that adequately capturing the direct impact of a single parameter is primordial to obtain an accurate surrogate model. The addition of pairwise interactions in the ℓ_2 sparse grid expansion only refines the shape of the probability distribution of NO predictions, with increased skewness and higher peak probability. The rate of the prompt initiation reaction has the largest relative contribution at the rich condition, but its contributions at the lean and stoichiometric conditions are also comparable to the contributions from the rate of the thermal initiation reaction. These findings suggest that the prompt initiation reaction, commonly known to be a key reaction for NO formation in rich flames, has significant contribution across equivalence ratios.

Traditional 2nd-order total-order expansions are also investigated to assess their capability to capture parameter interactions. The contribution analysis showed that although the most probable NO concentration can be estimated adequately, the pairwise variable interactions are inaccurate. Higher-order approximations or advanced tensor-product expansions should therefore be used to examine parametric relationship and perform inference to constrain the nitrogen and CH chemistry.

PERMISSION FOR USE

The content of this paper is copyrighted by Siemens Energy Canada Ltd. and is licensed to ASME for publication and distribution only. Any inquiries regarding permission to use the content of this paper, in whole or in part, for any purpose must be addressed to Siemens Energy directly.

ACKNOWLEDGMENT

The authors wish to acknowledge the support of the Natural Sciences and Engineering Research Council of Canada (NSERC), the Fonds de Recherche du Québec - Nature et Technologies and Siemens Energy Canada Limited.

REFERENCES

- [1] Versailles, P., Durocher, A., Bourque, G., and Bergthorson, J. M., 2019. “Nitric oxide formation in lean, methane-air stagnation flames at supra-atmospheric pressures”. *Proc. Combust. Inst.*, **37**(1), pp. 711–718.
- [2] Durocher, A., Bourque, G., and Bergthorson, J. M., 2020. “Quantifying the effect of kinetic uncertainties on NO predictions at engine-relevant pressures in premixed methane-air flames”. *J. Eng. Gas Turb. Power*, **142**(6).
- [3] Yousefian, S., Bourque, G., and Monaghan, R. F., 2018. “Uncertainty quantification of NO_x emission due to operating conditions and chemical kinetic parameters in a premixed burner”. *J. Eng. Gas Turb. Power*, **140**(12).
- [4] Hong, Z., Davidson, D. F., and Hanson, R. K., 2011. “An improved H₂/O₂ mechanism based on recent shock tube/laser absorption measurements”. *Combust. Flame*, **158**(4), pp. 633–644.
- [5] Hanson, R. K., 2011. “Applications of quantitative laser sensors to kinetics, propulsion and practical energy systems”. *Proc. Combust. Inst.*, **33**(1), pp. 1–40.
- [6] Klippenstein, S. J., 2017. “From theoretical reaction dynamics to chemical modeling of combustion”. *Proc. Combust. Inst.*, **36**(1), pp. 77–111.
- [7] Sheen, D. A., and Wang, H., 2011. “The method of uncertainty quantification and minimization using polynomial chaos expansions”. *Combust. Flame*, **158**(12), pp. 2358–2374.
- [8] Frenklach, M., Wang, H., and Rabinowitz, M. J., 1992. “Optimization and analysis of large chemical kinetic mechanisms using the solution mapping method-combustion of methane”. *Prog. Energy Combust. Sci.*, **18**(1), pp. 47–73.
- [9] Zsély, I. G., Zádor, J., and Turányi, T., 2008. “Uncertainty analysis of NO production during methane combustion”. *Int. J. Chem. Kinet.*, **40**(11), pp. 754–768.
- [10] Reagan, M. T., Najm, H., Pebay, P., Knio, O., and Ghanem, R., 2005. “Quantifying uncertainty in chemical systems modeling”. *Int. J. Chem. Kinet.*, **37**(6), pp. 368–382.
- [11] Najm, H. N., Debusschere, B. J., Marzouk, Y. M., Widmer, S., and Le Maître, O., 2009. “Uncertainty quantification in chemical systems”. *Int. J. Numer. Methods Eng.*, **80**(6-7), pp. 789–814.
- [12] Prager, J., Najm, H. N., Sargsyan, K., Safta, C., and Pitz, W. J., 2013. “Uncertainty quantification of reaction mechanisms accounting for correlations introduced by rate rules and fitted Arrhenius parameters”. *Combust. Flame*, **160**(9), pp. 1583–1593.
- [13] Lipardi, A. C., Versailles, P., Watson, G. M., Bourque, G., and Bergthorson, J. M., 2017. “Experimental and numerical study on NO_x formation in CH₄-air mixtures diluted with exhaust gas components”. *Combust. Flame*, **179**, pp. 325–337.
- [14] Durocher, A., Versailles, P., Bourque, G., and Bergthorson, J. M., 2020. “Impact of kinetic uncertainties on accurate prediction of NO concentrations in premixed alkane-air flames”. *Combust. Sci. Technol.*, **192**(6), pp. 959–985.
- [15] Glarborg, P., Miller, J. A., Ruscic, B., and Klippenstein, S. J., 2018. “Modeling nitrogen chemistry in combustion”. *Prog. Energy Combust. Sci.*, **67**, pp. 31–68.
- [16] Abian, M., Alzueta, M. U., and Glarborg, P., 2015. “Forma-

TABLE 4. EXPERIMENTALLY-MEASURED BOUNDARY CONDITIONS.

ϕ [–]	T_{in} [°C]	u_{in} [m/s]	V_{in} [1/s]	T_{surf} [°C]	P [atm]	l [mm]
0.8 (0.006)	81 (2.0)	0.582 (0.006)	60.5 (1.5)	69.9 (2.0)	1.000 (0.002)	10.153 (0.007)
1.0 (0.007)	82 (0.8)	0.838 (0.008)	95.2 (4.8)	115.4 (2.3)	1.000 (0.002)	9.653 (0.007)
1.3 (0.009)	81 (2.0)	0.600 (0.009)	65.3 (3.2)	90.4 (1.8)	1.000 (0.002)	9.739 (0.007)

tion of NO from N₂/O₂ mixtures in a flow reactor: toward an accurate prediction of thermal NO”. *Int. J. Chem. Kinet.*, **47**(8), pp. 518–532.

- [17] Thomsen, D. D., Kuligowski, F. F., and Laurendeau, N. M., 1999. “Modeling of NO formation in premixed, high-pressure methane flames”. *Combust. Flame*, **119**(3), pp. 307–318.
- [18] Lamoureux, N., El Merhubi, H., Pillier, L., de Persis, S., and Desgroux, P., 2016. “Modeling of NO formation in low pressure premixed flames”. *Combust. Flame*, **163**, pp. 557–575.
- [19] Watson, G. M., Versailles, P., and Bergthorson, J. M., 2016. “NO formation in premixed flames of C₁–C₃ alkanes and alcohols”. *Combust. Flame*, **169**, pp. 242–260.
- [20] Durocher, A., Meulemans, M., Versailles, P., Bourque, G., and Bergthorson, J. M., 2020. “Back to basics—NO concentration measurements in atmospheric lean-to-rich, low-temperature, premixed hydrogen–air flames diluted with argon”. *Proc. Combust. Inst.*
- [21] Rørtveit, G. J., Hustad, J. E., Li, S.-C., and Williams, F. A., 2002. “Effects of diluents on NO_x formation in hydrogen counterflow flames”. *Combust. Flame*, **130**(1-2), pp. 48–61.
- [22] Pillier, L., Idir, M., Molet, J., Matynia, A., and De Persis, S., 2015. “Experimental study and modelling of NO_x formation in high pressure counter-flow premixed CH₄/air flames”. *Fuel*, **150**, pp. 394–407.
- [23] Versailles, P., Watson, G. M., Lipardi, A. C., and Bergthorson, J. M., 2016. “Quantitative CH measurements in atmospheric-pressure, premixed flames of C₁–C₄ alkanes”. *Combust. Flame*, **165**, pp. 109–124.
- [24] Goodwin, D., Moffat, H., and Speth, R., 2016. Cantera: An object-oriented software toolkit for chemical kinetics, thermodynamics, and transport processes. <http://www.cantera.org>.
- [25] University of California at San Diego, 2005. Chemical-kinetic mechanisms for combustion applications. <http://combustion.ucsd.edu>. San Diego Mechanism web page, Mechanical and Aerospace Engineering (Combustion Research).
- [26] Versailles, P., Watson, G. M., Durocher, A., Bourque, G., and Bergthorson, J. M., 2018. “Thermochemical mechanism optimization for accurate predictions of CH concentrations in premixed flames of C₁–C₃ alkane fuels”. *J. Eng. Gas Turb. Power*, **140**(6).
- [27] Xiu, D., and Karniadakis, G. E., 2002. “The Wiener–Askey polynomial chaos for stochastic differential equations”. *SIAM J. Sci. Comput.*, **24**(2), pp. 619–644.
- [28] Adams, B., Bauman, L., Bohnhoff, W., Dalbey, K., Ebeida, M., Eddy, J., Eldred, M., Hough, P., Hu, K., Jakeman, J., Stephens, J., Swiler, L., Vigil, D., and Wildey, T., 2015. Dakota, A Multilevel Parallel Object-Oriented Framework for Design Optimization, Parameter Estimation, Uncertainty Quantification, and Sensitivity Analysis: Version 6.0 User’s Manual. Tech. rep., Sandia Technical Report SAND2014-4633.
- [29] Xiu, D., 2010. *Numerical methods for stochastic computations: a spectral method approach*. Princeton university press.
- [30] Smith, R. C., 2014. *Uncertainty Quantification: Theory, Implementation, and Applications*. Computational Science and Engineering, SIAM, Philadelphia.
- [31] Smolyak, S., 1963. “Quadrature and interpolation formulas for tensor products of certain classes of functions”. *Dokl. Akad. Nauk*, **148**(5), pp. 1042–1045.

APPENDIX A: Experimental boundary conditions

The experimentally-measured boundary conditions for the lean, stoichiometric, and rich conditions are provided in Table 4 for the equivalence ratio, ϕ , the inlet temperature, T_{in} , the inlet velocity, u_{in} , the inlet spread rate, $V_{in} = du/dz_{in}$, the stagnation surface temperature, T_{surf} , the pressure, P , and the numerical domain length, l . The uncertainty on the boundary conditions is shown in parentheses. Details regarding the equipment used, the measurement techniques, and the accuracy of these conditions have been reported by Watson and co-workers [19]. These boundary conditions are used to simulate the axisymmetric stagnation flames with the one-dimensional impinging jet model in Cantera 2.4 [24].